Article ID: 1000-324X(2016)05-0547-08 **DOI:** 10.15541/jim20150516

Isothermal Crystal Growth Behavior of $CaSiO_3$ in Ternary Oxide Melts

LIU Jing-Jing[1], HEULENS Jeroen[2], GUO Mu-Xing[1], MOELANS Nele[1]

(1. Department of Materials Engineering, KU Leuven, B-3001 Heverlee, Belgium; 2. Umicore Precious Metals Refining, B-2660 Hoboken, Belgium)

Abstract: The process of isothermal wollastonite ($CaSiO_3$) crystallization in the CaO-Al_2O_3-SiO_2 system was simulated using a phase field model coupled with the FACTSage Toxide thermodynamic database. The effects of composition and temperature on the crystallization behaviour were studied. The simulations show that for the considered cases, the wollastonite morphology is mainly determined by anisotropy in the interface energy and hardly affected by anisotropy in the interface kinetics. In agreement with the observations from *in-situ* experiments, the simulations show a transition from planar to dendritic growth with decreasing temperature and the dendritic structure becomes finer when the temperature is decreased in further. The growth rates and dendrite tip radii obtained in the simulations agree well with Ivanstov's theory and are of the same orders of magnitude as those measured experimentally.

Key words: crystal growth; morphology; $CaSiO_3$; phase field

During a typical continuous casting process, mold fluxes are continuously added on top of the mold. Mold fluxes are effective to keep a low friction between the mold and the liquid steel and control of heat transfer from steel strand to copper mould since the mold flux could melt, infiltrate the gap between the steel shell and the copper mold wall and form a flux film at the processing temperature. The following crystallization of this film might result in the formation of an air gap near the mould wall[1-2]. Therefore, large amounts of work have been focused on the crystallization of mold fluxes targeted for lubricating the strand, absorbing inclusions and moderating heat transfer during the continuous casting of steel[3-5]. In this specified area, the crystallization behavior of $CaSiO_3$ is of great importance. For instance, the morphology of $CaSiO_3$ particles has an obvious impact on the thermal resistance at the interface between mold flux film and copper mould. Crystallization of such a slag also influences the mineralogy of the cooled slag after tapping as well[6]. Therefore, a number of experimental techniques have been employed to investigate the behavior of slag crystallization[7-11]. Kashiwaya *et al*. first developed single/double hot thermocouple technology (SHTT/ DHTT) for *in-situ* observation and measurement of the crystallization of mould flux[7]. Orrling *et al*. found that the crystal morphology of mould flux was dependent on the degree of undercooling, as observed through confocal laser microscope (CSLM)[9]. Many achievements have been realized *via* advanced apparatus and elaborated experimental design. However, not all features of slag crystallization could be observed experimentally, amongst others because of the tremendous high growth rates of some crystals. Furthermore, it is very time consuming and costly to observe all these phenomena at high temperatures.

The phase field method has become a powerful approach for modelling complex morphology evolution[12]. Usually complex morphologies are found to form during crystallization, such as dendritic crystals. The phase field model was originally proposed for solidification in undercooled pure melts by Kobayashi[13] and was extended to binary alloys using WBM model by Wheeler, *et al*[14]. Steinbach, *et al* further extended the phase field approach from two-phase to multi-phase systems[15]. A framework for combining the phase field equations with diffusion equations and thermodynamic databases for multi-component systems was introduced by Tiaden, *et al*[16]. Our group recently developed a phase field model for multi-phase multi-component oxide systems coupled with Factsage databases[17]. Although the phase field method has been successfully applied to numerous applications, it is still a challenge to apply the phase-field method to multi-component systems and for realistic conditions. So far, only few simulations were performed of solidification in real ternary systems (and even

Received date: 2015-10-21; **Modified date:** 2015-12-05
Foundation item: High Performance Computer from VSC (Flemish Supercomputer Centrum)
Biography: LIU Jing-Jing (1983–), female, candidate of PhD. E-mail: jingjing.liu@mtm.kuleuven.be
Corresponding author: MOELANS Nele, professor. E-mail: nele.moelans@mtm.kuleuren.be

less for ternary oxide systems). Also the crystallization of crystals with hexagonal anisotropy, as is the case for wollastonite, has not been considered extensively so far.

In the present study, a phase field model with anisotropy in interfacial energy and kinetics, coupled with the FACTSage Toxide thermodynamic database[17], is used to study the isothermal crystallization behavior of $CaSiO_3$ in a typical mold flux. Besides the thermodynamic data, the other required input data, such as diffusion coefficients, interfacial energy, kinetics and anisotropy, are chosen as realistic as possible based on the available literature data. Several phase field simulations were carried out to assess the effect of composition and temperature on the growth morphology and kinetics of the wollastonite. The validity of the presented model and used input data is examined by comparing the simulated results with previous experimental observations[11].

1 Phase field model for multi-component systems

1.1 Governing equations

According to thermodynamic principles, microstructure evolution in a system at constant pressure, temperature and molar volume is driven by minimization of the total Gibbs energy. Two continuous non-conserved phase field variables η_{liquid} and η_{solid} were used to describe the microstructure of a system with two phases, namely solid and liquid. They characterize the physical state of the system at each position and time as follows: $\eta_{\text{liquid}}=1$, $\eta_{\text{solid}}=0$ for the liquid; $\eta_{\text{solid}}=1$, $\eta_{\text{liquid}}=0$ for the solid. At the solid-liquid interface, the η_{liquid} and η_{solid} vary smoothly between 0 and 1 over a small distance which is called the 'diffuse interface width'.

The total Gibbs free energy of the system (F) is assumed to consist of two contributions (Eq.1): chemical bulk (F_{chem}) and the interfacial free energy (F_{inter}), respectively.

$$F = F_{\text{inter}} + F_{\text{chem}} \tag{1}$$

The interfacial free energy is formulated as

$$F_{\text{inter}} = \int_v [m[(\frac{\eta_{\text{liquid}}^4}{4} - \frac{\eta_{\text{liquid}}^2}{2}) + (\frac{\eta_{\text{solid}}^4}{4} - \frac{\eta_{\text{solid}}^2}{2}) + 1.5\eta_{\text{liquid}}^2\eta_{\text{solid}}^2 + \frac{1}{4}] + \frac{\kappa}{2}[(\nabla\eta_{\text{liquid}})^2 + (\nabla\eta_{\text{solid}})^2]]\mathrm{d}V \tag{2}$$

Furthermore, the parameters κ and m are uniquely related to the interface energy (σ) and the diffuse interface width (l) assumed in the phase field model as $\sigma=(2m\kappa)^{1/2}/3$ and $l=(8\kappa/m)^{1/2}$.

The chemical bulk free energy has the form of

$$F_{\text{chem}} = \int_v (\phi_{\text{liquid}} f^{\text{liquid}} + \phi_{\text{solid}} f^{\text{solid}})\mathrm{d}V \tag{3}$$

Where the phase fractions ϕ_{liquid} and ϕ_{solid} are defined as

$$\phi_{\text{liquid}} = \frac{\eta_{\text{liquid}}^2}{\eta_{\text{liquid}}^2 + \eta_{\text{solid}}^2} \qquad \phi_{\text{solid}} = \frac{\eta_{\text{solid}}^2}{\eta_{\text{liquid}}^2 + \eta_{\text{solid}}^2} \tag{4}$$

The evolution equation for each phase field variable, η_i, follows a time-dependent Ginzburg-Laudau equation for non-conserved variables:

$$\frac{\partial\eta_i}{\partial t} = -L\frac{\delta F}{\delta\eta_i} \tag{5}$$

Where L is related to interface mobility (μ). Because our previous experiments[11] showed that the dendrite tip velocity was constant in time, it can be assumed that the growth of $CaSiO_3$ was bulk diffusion-controlled. Therefore, the value of L was chosen to obtain in the phase field model an interface velocity controlled by bulk diffusion in the liquid as described in Ref[18].

Following the approach of Kim-Kim-Suzuki[19], the interfacial region is considered as a mixture of the solid and liquid phase in equilibrium with each other. Phase compositions (x_k^i) are defined such that for each element the chemical potentials for the phase compositions in the solid and the liquid are equal, while the local mass balance is preserved:

$$\frac{\partial f^{\text{liquid}}}{\partial x_k^{\text{liquid}}} = \frac{\partial f^{\text{solid}}}{\partial x_k^{\text{solid}}} \tag{6}$$

$$x_k = \phi_{\text{liquid}} x_k^{\text{liquid}} + \phi_{\text{solid}} x_k^{\text{solid}} \tag{7}$$

A diffusion equation is derived for every independent component k:

$$\frac{\partial x_k}{\partial t} = \nabla\cdot[\phi_{\text{liquid}}(\sum_{l=1}^{c-1} M_{kl}^{\text{liquid}}\nabla\frac{\partial f^{\text{liquid}}}{\partial x_l^{\text{liquid}}}) + \phi_{\text{solid}}(\sum_{l=1}^{c-1} M_{kl}^{\text{solid}}\nabla\frac{\partial f^{\text{solid}}}{\partial x_l^{\text{solid}}})] \tag{8}$$

The elements M_{kl}^{liquid} form a diffusion mobility matrix M^{liquid} for the liquid phase, which relates to the interdiffusion matrix D^{liquid} and thermodynamic factors matrix G^{liquid} (the second derivatives of the Gibbs energy density with respect to the independent composition variables) according to the following formula (Eq.9).

$$D^{\text{liquid}} = M^{\text{liquid}} G^{\text{liquid}} \tag{9}$$

Since we consider isothermal growth and, based on our experimental observations, we assume that the growth of wollastonite is controlled by bulk diffusion, the mobility matrix M^{solid} for the solid phase does not affect the growth since there is no diffusion in the solid (the solid crystallizes at its equilibrium composition). In the simulations M^{solid} is therefore taken of the same order of magnitude as M^{liquid}, but with the off-diagonal elements equal to 0, to avoid the inaccuracies due to spurious solute trapping in phase-field models for solidification reported by Karma[20].

In summary, the morphological changes of the crystallizing $CaSiO_3$ can be simulated by solving equations (Eq. 5)

and (Eq. 8) under the constraints of equations (Eq. 6) and (Eq. 7).

1.2 Thermodynamic properties

The bulk thermodynamic properties of the liquid, such as Gibbs energy density f^{liquid}, diffusion potentials (the first derivatives of the Gibbs energy density with respect to the independent composition variables) and thermodynamic factors as a function of composition are retrieved from the FACTSage Toxide database through ChemApp as reported before[17].

Wollastonite is treated as a stoichiometric phase in the FACTSage Toxide database. Therefore, a parabolic Gibbs energy is constructed for the wollastonite phase based on Ref [17] such that the correct phase equilibria between this phase and the liquid phase are obtained and a minimal solubility exists in wollastonite to make it compatible with our continuum model formulation.

1.3 Anisotropy of the interface energy and interface kinetics

We assume that the anisotropy of the interface energy (σ) and interface mobility (μ) are of the form $\sigma = \sigma_0\lambda_\sigma(\theta)$ and $\mu = \mu_0\lambda_\mu(\theta)$ with θ the orientation of the interface. The model parameters are then taken according to Eq. (10a), (10b) and (10c):

$$\kappa = \kappa_0\lambda_\sigma(\theta) \tag{10a}$$

$$m = m_0\lambda_\sigma(\theta) \tag{10b}$$

$$L = L_0\lambda_\mu(\theta) \tag{10c}$$

with

$$\lambda_\sigma(\theta) = \lambda_\mu(\theta) = 1 + \delta\cos(a\theta) \tag{11}$$

σ_0 is the interfacial energy at θ =0, μ_0 is the interface mobility at θ =0, a is the mode of the anisotropy and δ is the strength of the anisotropy. Here, a=6 is taken due to the intrinsic hexagonal crystal structure of wollastonite.

The orientation of the interface (θ) can be derived at every position from the spatial variations of the order parameters representing the solid and the liquid as shown in Eq.12.

$$\theta = \arctan\left|\frac{\nabla_y\eta_{\text{liquid}} - \nabla_y\eta_{\text{solid}}}{\nabla_x\eta_{\text{liquid}} - \nabla_x\eta_{\text{solid}}}\right| \tag{12}$$

2 Experimental results

In-situ isothermal $CaSiO_3$ crystallization experiments have been performed for a Slag A with initial composition 42wt%CaO-48wt%SiO_2-10wt%Al_2O_3 (x_{CaO}^0=0.455, x_{Al2O3}^0= 0.06) and Slag B with initial composition 40.83wt%CaO-46.67wt%SiO_2-12.5wt%Al_2O_3 (x_{CaO}^0=0.447, x_{Al2O3}^0=0.075) at different temperatures using CSLM[11]. Based on thermodynamic calculations, these compositions were chosen from a composition domain where wollastonite is the only precipitating phase. The morphology of the wollastonite was found to be faceted with hexagonal symmetry for low undercooling. When the crystallization temperature was decreased, the morphology changed to dendritic with hexagonal symmetry. The dendrite tip velocity was found to be constant, in agreement with Ivanstov's theory. In CSLM experiments, the solidification occurs at the surface of the melt and the dendrite tip can be partially to fully submerge into the melt, depending on the values of the solid-liquid, solid-vapor and liquid-vapor tensions. The growth conditions at the tip can thus vary from closer to 2D, when the tip is only partially submerged, to close to 3D, when the dendrite tip is (almost) fully submerged. Comparison of the measured dendrite tip radii with those expected from the Ivantsov's theories in 2D and 3D, indicated that the growth conditions in the CSLM are indeed in between 2D and 3D.

3 Numerical implementation and simulation setup

3.1 Numerical implementation

The phase field and diffusion equations (Eq. 5 and 8) are discretized on an equidistant numerical grid using central finite difference. Adiabatic boundary conditions are implemented using ghost nodes at the border of the simulation domain. The program code was written in FORTRAN and executed on a High Performance Computer Cluster. Typical computation times on five ivybridge nodes, Xeon E5-2680v2 CPU@2.8 GHz with 64 GB RAM ranged from 72 h to 76 h for two dimensional simulations.

3.2 Simulation setup

In the simulations, the $CaSiO_3$ crystallization behaviour was studied in terms of morphology and growth behavior. The effects of composition and undercooling on these properties were investigated. Considering the six-fold morphological symmetry of $CaSiO_3$, as observed in the in-situ experiments, the simulation domain was limited to a quarter of the entire $CaSiO_3$ morphology. A nucleus of solid $CaSiO_3$ (x_{CaO}^0=0.499, x_{Al2O3}^0=0.002) was placed at the bottom-left corner of the simulation domain. All large-scale simulations were performed based on a square system with dimensions (1600×Δx) × (1600×Δy), over a time slot (t) of $2\times10^6\times\Delta t$. For the interface energy a typical value of σ_0 = 0.3J/m^2 was chosen. This value is comparable to Ja-Yong Choi, *et al*'s work[21], where interfacial tension between 42wt%CaO-48wt%SiO_2-10wt% Al_2O_3 slag and Al_2O_3 at 1873 K is around 0.45 J/m^2. The molar volumes of all components in the liquid and solid phase are assumed to be the same and constant. A mean value V_m = 23.6×10^{-6} m^3/mol was chosen based literature data[22]. No information on the strength of the anisotropy is available.

It is chosen as $\delta = 0.25$, which is the maximum value for which the interface stiffness is positive for all interface orientations. In a further study, the effect of the strength of the anisotropy will be considered for hexagonal symmetry. The other parameters were set as follows: grid size $\Delta x = \Delta y = 0.125\times10^{-7}$m, time step $\Delta t = 5\times10^{-7}$s and diffuse interface width of the phase field model $l = 8\Delta x$. The diffusion mobility matrix for $CaO\text{-}Al_2O_3\text{-}SiO_2$ used in the current simulations was calculated from the experimentally determined interdiffusion matrix[23] and the thermodynamic factor matrix that is calculated through ChemApp. In Suguwara's work[23], the temperature dependent expressions of interdiffusion coefficient were evaluated for a melt with composition 40wt%CaO-40wt% SiO_2 -20wt% Al_2O_3, which is close to the melts considered in the present simulations.

4 Simulation results and discussion

4.1 Wollastonite morphology

4.1.1 Effect of anisotropy on interface energy and interface kinetics

In the first set of simulations, both the interface energy anisotropy and interface kinetics anisotropy were considered using the forms shown in Eq. (10a) (10b) and (10c). Another set of simulations was performed only considering interface energy anisotropy (Eq. (10a) and (10b)). For each case, an evolution time of 1s was considered. The morphologies obtained in the different simulations for slag A at different temperatures, with anisotropy in the interface energy only and with anisotropy in both interface energy and interface kinetics are shown in Fig. 1(a)-(b) and Fig. 1(c)-(d), respectively. These simulations show that, in the presence of anisotropy in interface energy and when growth is controlled by bulk diffusion in the liquid, the morphology of the growing wollastonite is hardly affected by anisotropy in interface kinetics. Similar phenomena were also reported in Brener's work[24]. This finding is also in agreement with Kirkpatrick's work[25] where it is stated that for most silicates the morphology is mainly governed by anisotropy in interface energy. This correspondence again indicates that it is reasonable to assume that wollastonite growth is diffusion controlled. Based on these findings, we only considered the interface energy anisotropy in the following simulations.

4.1.2 Effect of the crystallization temperature

The simulated shapes of isothermally crystallized wollastonite, at different undercoolings for slag A and slag B are presented in Fig. 2(a)-(c) and Fig. 3(a)-(c), respectively. The results show a transition from growth with a flat solid-liquid interface at low undercooling (Fig. 2(a)/Fig. 3(a)) to dendritic (Fig. 2(b)-(c)/Fig. 3(b)-(c)) at larger undercooling.

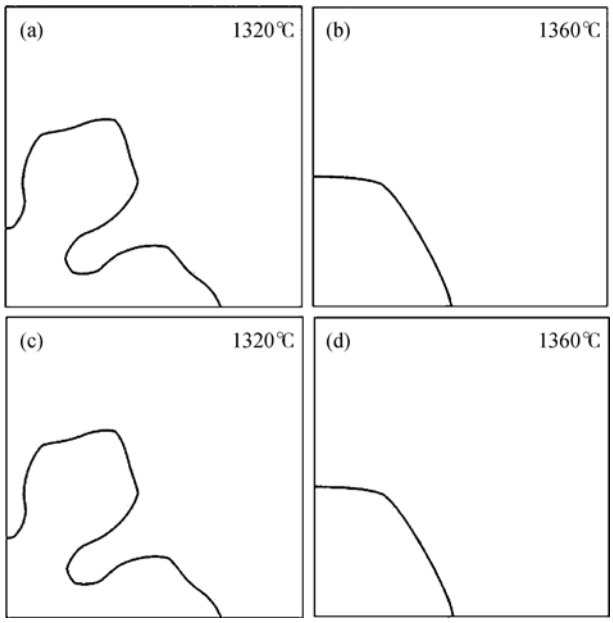

Fig.1 Simulated morphologies of wollastonite at t=1 s for slag A at (a) 1320℃; (b) 1360℃ with anisotropy in the interface energy only (c) 1320℃ and (d) 1360℃ with anisotropy in interface energy and interface kinetics

With a further decrease of the crystallization temperature, the dendritic structure becomes finer (Fig. 2(c)/Fig. 3(c)). This tendency is qualitatively in good agreement with our experimental observations**,** as shown in Fig. 2(d)-(f) and Fig. 3(d)-(f). However, the temperature at which the transition occurs deviates from the experimental. For example, for slag A, the transition from flat to dendritic is around 1340℃ in the simulations, whereas it is around 1390℃ in the experiments. Possible reason for these deviations between experiments and simulations is the intrinsic errors in the experimentally determined temperatures. Considering the samples during CSLM observation were heated by radiation and the low thermal conductivity of CaO based slags, the temperature measured by the thermocouple beneath the sample may deviate from the real temperature on the specimen surface.

A similar tendency was observed in the simulations for slag B (Fig. 3(a)-(c)), although the transition temperature is different.

The transition from a flat to dendritic growth with decreasing temperature can be primarily explained by an instability of the planar interface due to the larger driving force for crystallization at higher undercoolings.

4.2 Dendritic wollastonite growth

From the 0.5 contours of the η_{liquid}, a set of points are generated for a selected number of time steps as shown in Fig. 4(a). Through these points, a second order polynomial was fitted, which is further used to determine the radius and the position of the dendrite tip. The second order

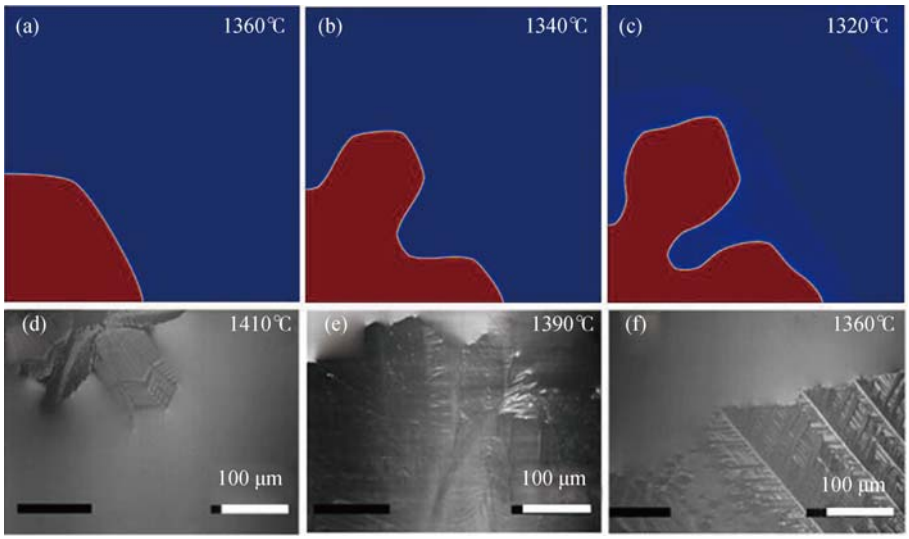

Fig. 2 Simulated and experimental morphologies of wollastonite for different undercoolings for slag A: (a) Δ=65℃; (b) Δ=85℃; (c) Δ=105℃ after a simulation time of 1 s and (d) Δ=15℃; (e) Δ=35℃; (f) Δ=65℃ observed in the experiments

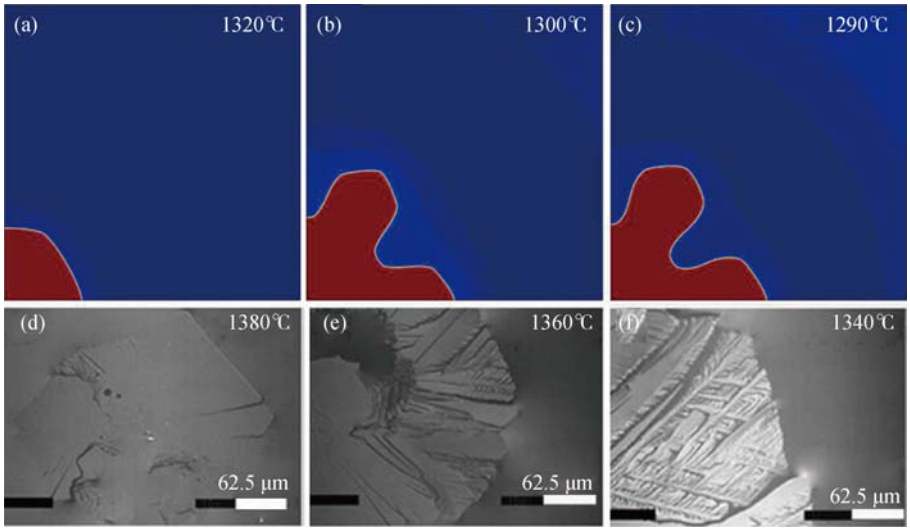

Fig. 3 Simulated and experimental morphologies of wollastonite for different undercoolings for slag B: (a) Δ=60℃; (b) Δ=80℃; (c) Δ=90℃ after a simulation time of 1 s and (d) Δ=0℃; (e) Δ=20℃; (f) Δ=40℃ observed in the experiments

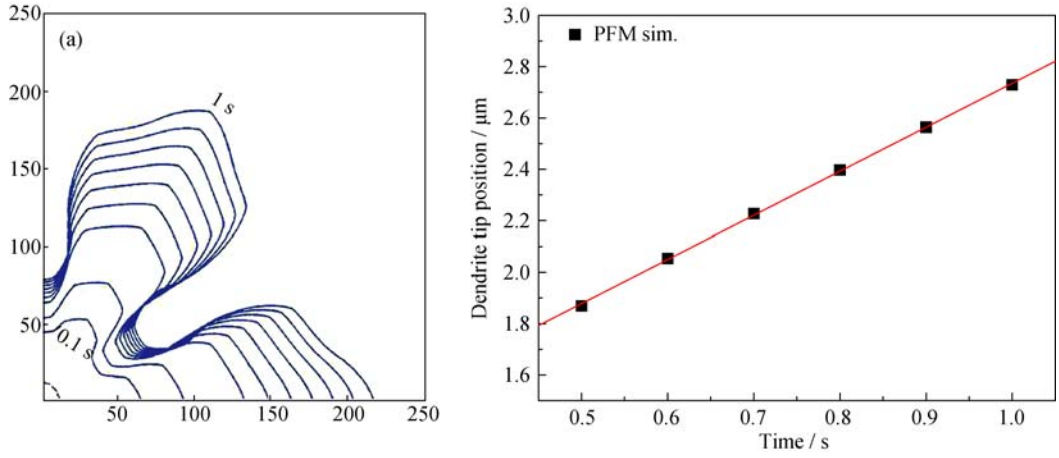

Fig. 4 (a) The simulated dendrite in slag A at 1320℃ is presented by means of the 0.5 contour of η_{liquid} for different time steps, (b) dendrite tip position as a function of time. The dendrite tip velocity is determined as the slope of this line

polynomial is intentionally chosen due to its similarity with Ivanstov's parabolic solution. The dendrite tip velocity is determined from the slope of the line, which represents the position of the dendrite tip as a function of time, as illustrated in Fig. 4(b).

As described in our previous paper[11], the slope of the dendrite tip position as a function of time is taken as the growth rate of the dendrite. The experimentally determined growth rates of the wollastonite approach a constant value. Also in the simulations, we find a constant growth rate in all cases. For example, as shown in Fig. 4(b), the dendritic tip approaches a constant velocity of 1.71 μm/s in slag A at 1320℃.

The growth rates obtained in the two-dimensional simulations for different undercoolings for slag A and slag B are plotted in Fig. 5(a). The dendrite tip velocities for slag A are 1.62 μm/s and 1.71μm/s in the simulations at an undercooling of 85℃ and 105℃, respectively. For slag B, dendrite tip velocities of 1.25 μm/s and 1.52 μm/s were obtained in the simulations for an undercooling of 80℃ and 90℃. For both slags, the experimental and simulated velocities are of the same order. Apparently, in both cases the experimental velocities are slightly higher than those obtained in the two-dimensional simulations. The agreement for slag B seems to be much better than for slag A.

The simulated wollastonite dendritic tip radii at different undercoolings are plotted in Fig. 5(b). For slag A, a dendrite tip radius of 0.628 μm and 0.366 μm was found for an undercooling of 85℃ and 105℃, respectively. For slag B, tip radii of 0.574 μm and 0.497μm were found for undercoolings of 80℃ and 90℃, respectively. In Fig. 5(b), the dendrite tip radii obtained from the simulated microstructures are compared with those obtained from the experiments. In agreement with experiments, for both slags, a smaller dendrite tip radius is obtained at a higher undercooling in the simulations. However, the dendrite tip radii obtained in the simulations are smaller than those obtained from the CSLM results.

According to Ivanstov's theory, the dendrite tip velocity (v) and radius (ρ) at steady state growth is related to the Peclet number (P), as shown in Eq.13.

$$P = \frac{\rho v}{2D} \tag{13}$$

For a given supersaturation Δ of the melt, the Peclet number (P) is determined by the following Ivanstov formulas in 2D and 3D:

$$\Delta = \sqrt{\pi P_{2D}}\exp(P_{2D})\mathrm{erfc}(\sqrt{P_{2D}}) \tag{14a}$$

$$\Delta = P_{3D}\exp(P_{3D})Ei(P_{3D}) \tag{14b}$$

According to Eq. 14, for a given composition and undercooling Δ, the Peclet number P, and therefore, for a given diffusion coefficient D, ρv are determined based on Eq. 13 and Eq. 14. In Fig. 6, we compare the ρv values as obtained from the simulations with those obtained from the experiments and the solutions of the 2D and 3D Ivanstov theory. The ρv values obtained in the 2-dimensional simulations are close to those obtained from Ivantsov's relation for 2D, indicating that the numerical implementation of the phase-field equations is accurate, the numerical parameters are chosen well and that the spurious solute trapping effects, often present in phase-field simulations, are negligible in our simulations. There is small deviation for the small tip radius (slag A, at 105℃ undercooling) because the effect of interfacial energy is not included in Ivanstov theory, while it is considered in the simulations. The experimental values are in between the solutions from the 2D and 3D Ivantsov's relations (Eq. 14a and Eq. 14b). There are two main reasons for these deviations between experiments and simulations.

(1) In the CSLM experiments, it is only possible to observe crystals growing on the surface of the melt. As mentioned in section 3, depending on the three interfacial tensions (of the solid-liquid, solid-vapor and liquid-vapor

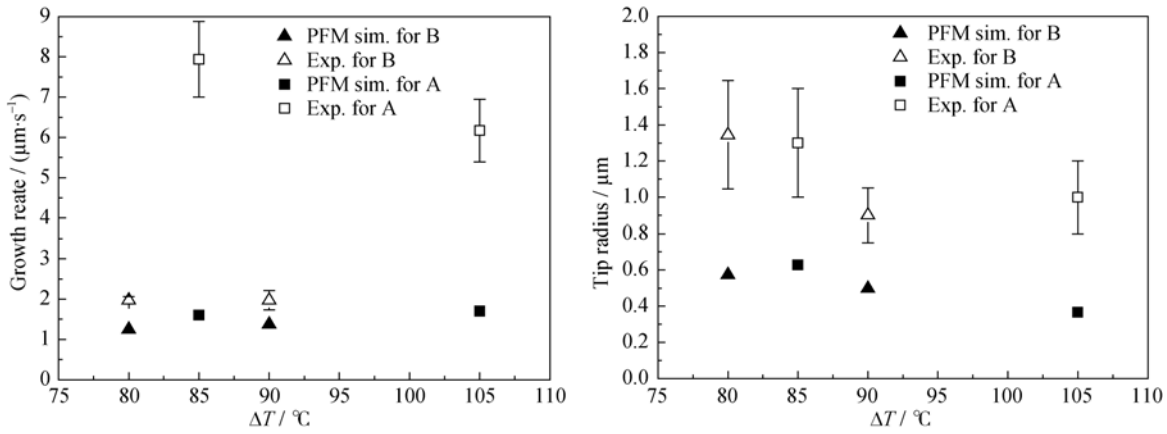

Fig. 5 (a) Dendrite tip velocity and (b) radius of wollastonite dendrite as a function of the undercoolings. The data of phase field simulations (filled mark) are shown in comparison with experimental data (open mark)

interfaces), the dendrite tip may be partially submerged in the liquid, resulting in growth behaviour that follows closely solidification theories in 2D, or (almost) fully submerged, resulting in growth behaviour following 3D solidification theories. Since, interfacial energies are a function of composition and temperature, these conditions may be different for different compositions and at different temperatures. In the simulations, however, growth in 2D is assumed. In Fig. 6, it can be seen that the values of ρv obtained from the simulations are indeed close to those obtained from Ivantsov's relation for 2D, whereas the experimental data are all in between the two values obtained from Ivantsov's relations for 2D and 3D. Although comparison with CSLM observations has some difficulties (*e.g.* solidification at the surface and it is not clear how much the dendrite tip is submerged), it is state of the art technique for the *in-situ* observation of high temperature phenomena, which enables precise temperature history and atmosphere control and high resolution observation. The latter is of significant importance to directly measure dendrite tip velocity. Other techniques such as Single (or Double) Hot Thermocouple Technique (SHTT or DHTT) can only obtain a relatively low resolution images and evaluates the solidified solid area as a function of time (but impossible for dendrite tip velocity measurement).

(2) The diffusion coefficients for the liquid were evaluated from the temperature dependent expression[23] determined based on diffusion coefficient measurements for a slag with composition 40wt%CaO-40wt%SiO_2-20wt%Al_2O_3. It is well known that the interdiffusion coefficient is composition dependent and especially for slag A, the composition deviates from that of the CaO-Al_2O_3-SiO_2 slag for which the diffusion matrix was calculated[23]. Using

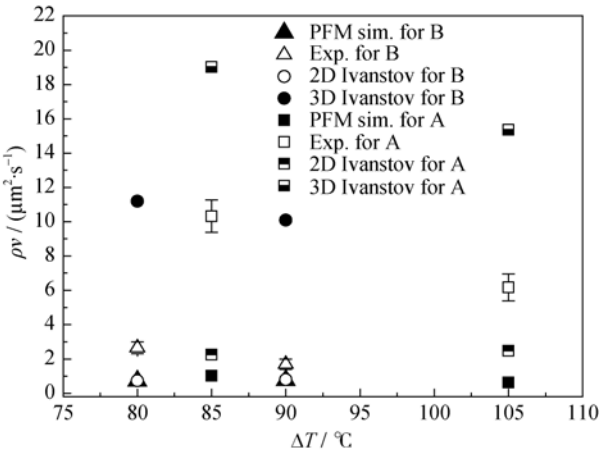

Fig. 6 Products of dendrite tip velocity and radius as a function of the undercoolings. The data of phase field simulations are shown in comparison with experimental data and the solutions from the 2D and 3D Ivantsov relations. The ρv values obtained from the simulations for slag B overlap with those obtained from the 2D Ivanstov equation

Urbain model[26], the viscosity calculated for slag A is smaller than that calculated for the slag with composition considered[23] to determine the diffusion coefficients. Based on the Einstein-Stokes equation[27], the magnitude of the diffusion coefficients is typically inversely proportional to the viscosity. Therefore, we expect that the real diffusion coefficients of slag A might be larger than the values we have used in the simulations. To verify the effect of a larger diffusion coefficient on the simulation results for slag A, another simulation was performed for slag A at 1320℃ using a diffusion coefficient matrix with all values 10% larger than the original values. From this simulation, a ρv value equal to 1.2 $\mu m^2/s$ instead of 0.625 $\mu m^2/s$, was obtained, which is closer to the experimental value (6.17±0.78) $\mu m^2/s$. Obviously, the gap between the experimental and simulated results will be smaller if a higher coefficient value of slag A is used.

5 Conclusion

In this work, the process of isothermal $CaSiO_3$ crystallization in CaO-Al_2O_3-SiO_2 systems is simulated by a phase field model. The effects of composition and temperature on isothermal $CaSiO_3$ crystallization behaviour were considered. The simulated wollastonite crystal structures were compared with the structures observed by CSLM at the same compositions and cooling conditions. The dependence of the morphology evolution, dendrite tip velocity and dendrite tip radius on composition and undercooling were analysed. Several conclusions could be drawn from this work:

1) The morphology of wollastonite during isothermal crystallization is governed by anisotropy in interface properties.

2) As temperature decreases, the morphology of $CaSiO_3$ varies from flat to dendritic. For a further decrease in temperature, the dendrite tip becomes sharper, which is in agreement with the experimental results.

3) The simulated growth rates and dendrite tip radii are of the same order as those measured experimentally, but there are some deviations due to differences in the experimental and simulated conditions and inaccuracies in the input data used for the simulations.

The presented simulations account very precisely for thermodynamic effects in ternary systems and also quite accurately for the diffusion properties and their composition dependence. Based on the experimental observations, we have assumed anisotropic interfacial properties with hexagonal symmetry. However more experimental information is required on the values of the interfacial energies and interface kinetics as a function of interface orientation to increase the accuracy of the simulations further.

References:

[1] SARASWAT R, MAIJER D M, LEE P D, *et al*. The effect of mould flux properties on thermo-mechanical behaviour during billet continuous casting. *ISIJ Int.*, 2007, **47:** 95–104.

[2] KAJITANI T, OKAZAWA K, YAMADA W , *et al*. Cold model experiment on infiltration of mould flux in continuous casting of steel: simple analysis neglecting mould oscillation. *ISIJ Int.,* 2006, **46:** 250–256.

[3] STONE D T, THOMAS B G. Measurement and modelling of the heat transfer across interfacial mold flux layers. *Can. Metall. Q.*, 1999, **38(5):** 363–375.

[4] ZHANG Z T, LI J, LIU P. Crystallization behavior in fluoride-free mold fluxes containing TiO_2/ZrO_2. *J. Iron Steel Res. Int.* , 2011, **18:** 31–37.

[5] CHO J, SHIBATA H. Effect of solidification of mold fluxes on the heat transfer in casting mold. *J. Non-Cryst. Solids,* 2001, **282:** 110–117.

[6] CAO J W, WANG Z. Effect of Na_2O and heat-treatment on crystallization of glass–ceramics from phosphorus slag. *J. Alloys Compd.*, 2013, **557:**190–195.

[7] KASHIWAYA Y, CICUTTI C E, CRAMB A W, *et al.* An investigation of the crystallization of a continuous casting mold slag using the single hot thermocouple technique. *ISIJ Int.*, 1998, **38:** 348–356.

[8] JONES P, DESMET D, GUO M, *et al.* Using confocal scanning laser microscopy for the *in situ* study of high-temperature behaviour of complex ceramic materials.*J. Eur. Ceram. Soc.*, 2007, **27(12):** 3497–3507.

[9] ORRLING C, SRIDHAR S, CRAMB A W. *In situ* observation of the role of alumina particles on the crystallization behavior of slags. *ISIJ Int.*, 2000, **40:** 877–885.

[10] HEULENS J, BLANPAIN B, MOELANS N. Analysis of the isothermal crystallization of $CaSiO_3$ in a $CaO-Al_2O_3-SiO_2$ melt through *in situ* observations. *J. Eur. Ceram. Soc.*, 2011, **31(10):** 1873–1879.

[11] LIU J , CHEN G, YAN P, *et al. In-situ* observation of isothermal $CaSiO_3$ crystallization in $CaO-Al_2O_3-SiO_2$ melts: a study of the effects of temperature and composition. *J. Cryst. Growth,* 2014, **402:** 1–8.

[12] MOELANS N, BLANPAIN B, WOLLANTS P. An introduction to phase-field modeling of microstructure evolution. *Calphad*, 2008, **32(2):** 268–294.

[13] KOBAYASHI R. Modeling and numerical simulations of dendritic crystal growth. *Physica D*, 1993, **63(3/4):** 410–423.

[14] WARREN J A, BOETTINGER W J. Prediction of dendritic growth and microsegregation patterns in a binary alloy using the phase-field method. *Acta Metall Mater,* 1995, **43(2):** 689–703.

[15] STEINBACH I, PEZZOLLA F, NESTLER B, *et al.* A phase field concept for multiphase systems. *Physcia D*, 1996, **94:** 135–147.

[16] TIADEN J, NESTLER B, DIEPERS H J, *et al.* The multi-phase-field model with an integrated concept for modelling solute diffusion. *Physcia D*, 1998, **115:** 73–86.

[17] HEULENS J, BLANPAIN B, MOELANS N. A phase field model for isothermal crystallization of oxide melts. *Acta Mater.*, 2011, **59(5):** 2156–2165.

[18] MOELANS N. A quantitative and thermodynamically consistent phase-field interpolation function for multi-phase systems. *Acta Mater.*, 2011, **59(3):** 1077–1086.

[19] KIM S G, KIM W T, SUZUKI T. Phase-field model for binary alloys. *Phys. Rev. E*, 1999, **60:** 7186–7197.

[20] KARMA A. Phase-field formulation for quantitative modeling of alloy solidification. *Phys. Rev. Lett.,* 2001, **87:** 115701/1–4.

[21] CHOI J Y, LEE H G. Wetting of solid Al_2O_3 with molten $CaO-Al_2O_3-SiO_2$. *ISIJ Int.*, 2003, **43:** 1348–1355.

[22] COURTIAL P, DINGWELL D B. Nonlinear composition dependence of molar volume of melts in the $CaO-Al_2O_3-SiO_2$ system.*GEOCHIM COSMOCHIM AC*, 1995, **59(18):** 3685–3695.

[23] HEULENS J, NAGATA K. Interdiffusivities matrix of $CaO-Al_2O_3-SiO_2$ melt at 1723 K to 1823 K. *Metall. Mater. Trans. B*, 2011, **42(6):** 1080.

[24] RENER E A. Effects of surface energy and kinetics on the growth of needle-like dendrites. *J. Cryst. Growth*, 1990, **99(1–4):** 165–170.

[25] KIRKPATRICK R J. Crystal growth from the melt: a review. *Am. Mineral.,* 1975, **60:** 798–814.

[26] NAKAMOTO M, LEE J, TANAKA T. A model for estimation of viscosity of molten silicate slag. *ISIJ Int.*, 2005, **45(5):** 651–656.

[27] EDWARD J T. Molecular volumes and the Stokes-Einstein equation. *J. Chem. Educ.*, 1970, **47(4):** 261.

硅灰石晶体在三元氧化物熔体中的生长行为研究

刘晶晶[1], HEULENS Jeroen[2], GUO Mu-Xing[1], MOELANS Nele[1]

(1. Department of Materials Engineering, KU Leuven, B-3001 Heverlee, Belgium; 2. Umicore Precious Metals Refining, B-2660 Hoboken, Belgium)

摘 要: 利用耦合 FACTSage Toxide 热力学数据库的定量相场模型, 本研究模拟了硅灰石($CaSiO_3$)在 $CaO-Al_2O_3-SiO_2$ 体系中的恒温晶体生长过程, 并研究了熔体组分和温度对 $CaSiO_3$ 结晶过程的影响。结果表明, 硅灰石的形貌主要由其表面能的各向异性所决定, 而几乎不受界面动力学的各向异性所影响。此外, 随着温度的降低, 析出的硅灰石的生长方式由平面生长向枝晶生长方式转变, 于此同时, 更加精细的枝晶结构也逐渐呈现出来。模拟所得的枝晶生长速度和尖端半径与 Ivanstov 理论所得结果一致, 和实验测得的数据也处于同一数量级。

关 键 词: 晶体生长; 形貌; 硅灰石; 相场

中图分类号: TQ174 **文献标识码:** A